Validation of Parameteric Directional MIMO Channel Models from Wideband FDTD Simulations of a Simple Indoor Environment *

*Jon W. Wallace and Michael A. Jensen

Department of Electrical and Computer Engineering,
459 CB, Brigham Young University, Provo, UT 84602-4099,
wall@ieee.org, jensen@ee.byu.edu

1 Introduction

Accurate modeling of multiple-input multiple-output (MIMO) wireless channels is an important research area, since capacity computations and algorithmic assessment depend on accurate channel models. The double-directional model [1] is an elegant extension of previous single-directional parametric modeling efforts [2]. This method assumes that scatter is "specular," or that the channel response can be decomposed into plane or spherical wave components (referred to as "rays"), allowing parametric techniques to be applied [3]. A "diffuse" channel, however, refers to one in which the plane wave assumption is violated. Rough surfaces, near-field scatter, and diffraction all lead to a diffuse channel. Application of parametric methods to diffuse channels may lead to erroneous conclusions [4].

We assess the specularity of the indoor channel through wideband two-dimensional (2D) finite-difference time-domain (FDTD) simulations of a simplified environment. The geometry presents a lower bound on how diffuse the environment is, since the inclusion of furniture, duct work, and rough walls likely reduces channel specularity. We achieve reconstruction accuracy between 70%-90% for this environment with a simple CLEAN-like deconvolution algorithm. Further, error in the capacity of reconstructed channels over 250 MHz of bandwidth is only 1%-6%. These results suggest that parametric models may still be very useful for indoor MIMO modeling, even though diffuse scattering is present.

2 FDTD Simulations

The FDTD method was chosen for ease of implementation and its ability to capture all important scattering mechanisms. Full-wave modeling is necessary, since tools such as ray-tracing inherently assume a plane wave model. Two-dimensional simulations were chosen due to computer memory constraints.

Figure 1 depicts the FDTD simulation area, where only the cinder block walls (homogeneous dielectric with $\epsilon_r = 2$) and supporting beams (solid perfect conductors) are included. A center frequency of 2.45 GHz was assumed, and the region was discretized at a spatial resolution of 10 cells per wavelength. Numerical dispersion was virtually eliminated with a fourth order approximation of the central finite-differences and a time resolution of 32 steps per period. The transmit array was a 19-element cross consisting of two superimposed 8-element uniform linear arrays (ULAs) with $\lambda/8$ inter-element spacing. Each transmit antenna required a separate FDTD simulation with a vertical ($\hat{z}$) electric current source at the antenna position. The excitation signal was a Gaussian pulse ($\sigma = 0.707T$, where T is the sinusoidal period) modulated with the 2.45 GHz sine wave, yielding about 2 GHz of usable probing bandwidth. Simulations were run for $300T$, at which point all significant energy had left the simulation domain. The $\hat{z}$-directed electric field intensity (E_z) was stored on

*This work was supported by the National Science Foundation under Wireless Initiative Grant CCR 99-79452 and Information Technology Research Grant CCR-0081476.

a Cartesian grid with 0.2λ steps over the complete simulation time. For double-directional estimation, an 11×11 element uniform rectangular array (URA) was formed at the receiver with 0.4λ inter-element spacing.

Figure 2 plots the equivalent baseband E_z fields when the center transmit antenna is excited at times $t = 70$ and $t = 140$, demonstrating strong guiding by the hallway and large transmission through walls.

3 Double-Directional Reconstructions

A variety of parametric estimation techniques are available [3] which have simple double-directional extensions. Since the purpose of this work is to assess the specularity of the channel, and not the efficiency or accuracy of any particular method, we chose a method that is not only conceptually simple, but also robust and very flexible. This method is very similar to the CLEAN algorithm [2] and is essentially a conditional maximum-likelihood estimator. Arrivals are found by correlating the channel response with the analytical response of the channel to a single ray (a planar or spherical wave component). A numerical optimization finds the best correlation over the component parameters: angle of arrival (AOA), angle of departure (AOD), and curvature (C), where $C = 1/d$, and d is distance to the spherical wave source in wavelengths. The correlation value at the optimized parameters gives the arrival amplitude and phase. Finally, the response of the arrays to the single component is computed and subtracted from the complete response. The process continues until some minimum error or maximum arrival limit is reached. RMS error (ξ) of the reconstructed field is defined as $\xi^2 = (\sum_k |f_k^{\mathrm{R}} - f_k^{\mathrm{A}}|^2)/(\sum_k |f_k^{\mathrm{A}}|^2)$, where f_k^{A} and f_k^{R} are the kth actual and reconstructed field components, respectively. In this work, the CLEAN algorithm was run until either $\xi < 0.1$ or 100 rays were found.

Figure 3 shows a typical run of the algorithm on data generated with the double-directional Saleh-Valenzeula Angular (SVA) model [2, 5], where Gaussian noise has been added to achieve 30 dB SNR for the time-domain signal. The array geometries and simulated time-domain signals coincide with those in the FDTD simulations. We chose curvature C according to an i.i.d. uniform distribution on $[0, 0.1]$. For this example, 98 of the 123 arrivals were found, and RMS reconstruction error was 9%. RMS error for the estimates of arrival time, arrival/departure angle, and arrival/departure curvature were $0.02T$, 0.2°, and $0.01/\lambda$, respectively, representing excellent agreement. Application of ESPRIT-type estimators yielded inferior performance, likely due to dense arrivals and the bandwidth limitation required for ESPRIT.

Double-directional parameter estimation was performed at the numbered locations in Figure 1. Due to restricted space, we will concentrate mainly on Location 18. Here, a metal beam obstructs the quasi line-of-sight (LOS) component. In the other positions, a much stronger quasi-LOS component was present. Figure 4 plots the times of arrival, angles of departure and arrival, and relative amplitude. By inspection of the time-domain simulations, the estimated rays could be correlated with scattering objects to produce Figure 5.

Important observations can be made from maps such as Figure 4. First, arrivals cluster around obvious scattering objects, even though the environment is mainly straight walls. This diffuse behavior might result from scattering objects of finite extent or slight errors in the CLEAN algorithm at each step. Second, when a strong LOS or quasi-LOS component is present, specular components with only 0-2 bounces are significant. When LOS is completely obstructed, 1-3 bounces are significant. Finally, significant scattering objects not only occur near the transmit and receive arrays, but also in the space inbetween. This raises questions as to the applicability of ring-type models for the indoor channel.

Pos	1	2	4	5	6	7	9	11	12	13	14	17	18	19	Mean
ξ_c	13.7	10.7	11.5	13.7	18.0	28.7	15.6	28.1	32.0	18.7	13.7	20.7	28.9	16.9	18.2
ξ_p	14.6	14.1	12.9	14.5	19.0	29.3	16.3	28.4	32.7	18.9	14.7	20.8	29.5	17.2	19.3
ξ_H	11.6	9.3	9.1	12.0	17.2	32.2	15.0	24.0	33.0	18.5	11.2	17.7	29.0	14.7	17.2
C_a	37.5	35.2	33.3	32.0	36.2	45.7	34.7	37.6	42.6	36.6	39.0	33.6	44.8	32.8	36.7
C_c	36.4	35.0	32.8	30.3	34.0	42.2	33.7	34.8	40.5	35.4	37.1	31.5	42.2	31.2	35.0
C_p	36.5	35.1	32.5	30.2	33.9	42.1	33.7	34.7	40.5	35.5	37.1	31.4	42.2	31.2	35.0
Err	2.9	0.5	1.5	5.6	6.2	7.7	2.9	7.5	5.0	3.3	4.8	6.5	5.8	4.8	4.6

Table 1: Reconstruction error (ξ) and capacity (C), and mean values over all 19 locations. Some locations are omitted for brevity.

Table 1 lists reconstruction error, where ξ_c and ξ_p are the percent RMS error in the reconstructed time-domain response waveform with a spherical wave or plane wave basis, respectively, and ξ_H is the error in the channel transfer matrix for a spherical wave basis over 250 MHz of bandwidth. Error is lowest when strong LOS or quasi-LOS is present.

4 Capacity Computations

The effect of parametric reconstruction error on capacity is of interest. Here, average capacity is computed for each position with the water-filling solution over 250 MHz of bandwidth assuming a receive SNR of 20 dB. Arrays were chosen to coincide with the FDTD simulations. The transmit array was a 9-element cross (two 4-element ULAs with $\lambda/2$ inter-element spacing), and the receiver was a 4×4 URA with 0.4λ inter-element spacing.

Table 1 lists capacity of the actual channel response (C_a), capacity of reconstructions with a spherical wave basis (C_s) or plane wave basis (C_p), and the percent difference between C_s and C_a (Err). Very small error in capacity of reconstructed channels is evident. Also plane and spherical wave reconstructions yield similar performance.

Figure 6 plots the convergence of the capacity as a function of the number of rays. In producing Figure 6, we have sorted the rays in terms of decreasing amplitude. At all locations, an obvious "knee" was present in the capacity convergence curves at about 20 rays, at which point at least 75% of the actual capacity was captured.

References

[1] M. Steinbauer, A. F. Molisch, and E. Bonek, "The double-directional radio channel," *IEEE Antennas and Propagation Magazine*, vol. 43, pp. 51–63, Aug. 2001.

[2] Q. H. Spencer, B. D. Jeffs, M. A. Jensen, and A. L. Swindlehurst, "Modeling the statistical time and angle of arrival characteristics of an indoor multipath channel," *IEEE Journal on Selected Areas in Communications*, vol. 18, pp. 347–360, Mar. 2000.

[3] H. Krim and M. Viberg, "Two decades of array signal processing research: the parametric approach," *IEEE Signal Processing Magazine*, vol. 13, pp. 67–94, July 1996.

[4] M. Bengtsson and B. Volcker, "On the estimation of azimuth distributions and azimuth spectra," in *IEEE VTC'2001 Fall Conf.*, vol. 3, (Atlantic City, NJ), pp. 1612–1615, Oct. 7-11 2001.

[5] J. W. Wallace and M. A. Jensen, "Modeling the indoor MIMO wireless channel," *IEEE Transactions on Antennas and Propagation*, vol. 50, pp. 591–599, May 2002.

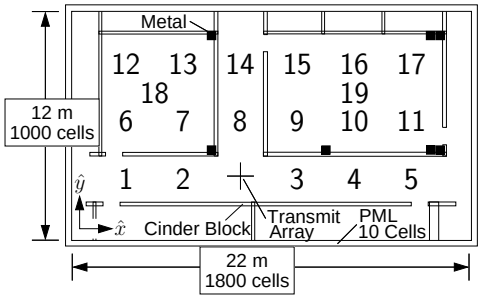

Figure 1: Simulation area (cinder block, metal beams) and estimation locations

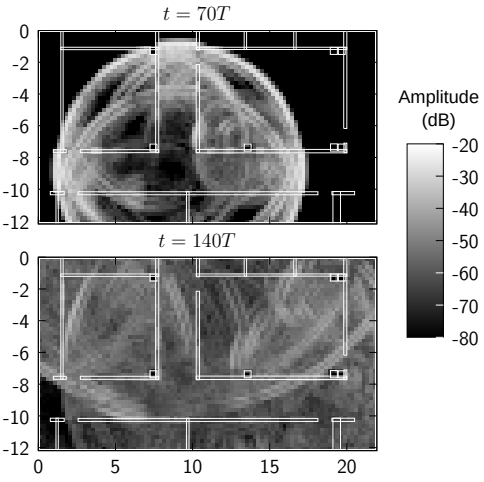

Figure 2: Baseband time-domain E_z fields at simulation times $t = 70T$, and $t = 140T$, where T is the sinusoidal period

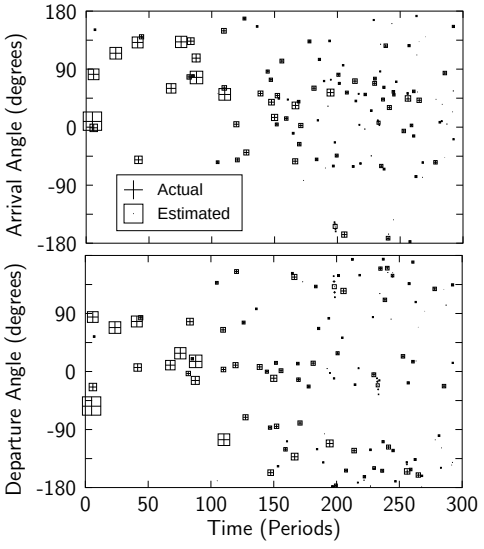

Figure 3: Example run of the CLEAN algorithm. Symbol size is proportional to amplitude in dB on the range $[-25, 0]$ dB.

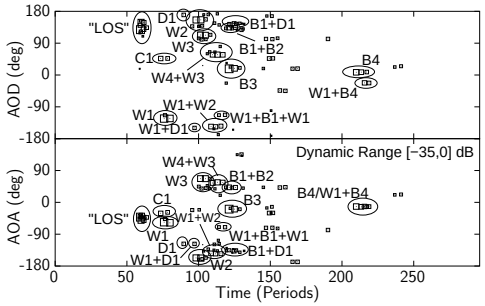

Figure 4: Angles of arrival and departure, and times of arrival for Location 18. Symbol size is proportional to amplitude in dB on the range $[-35, 0]$ dB. See Figure 5 for object identifiers.

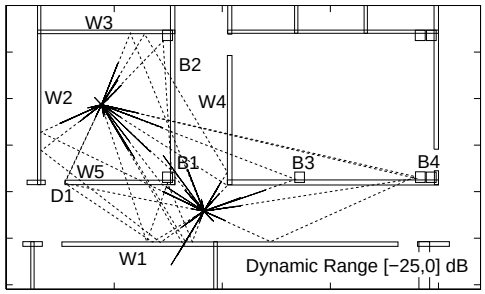

Figure 5: Observed scatterers for Location 18. Length of solid rays is proportional to amplitude in dB on the range $[-25, 0]$ dB. Dashed lines show observed propagation paths. Object identifiers are W for walls, B for beams, and D for doorways.

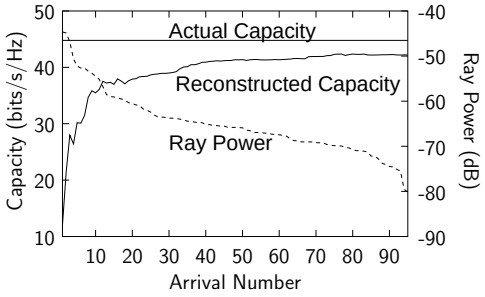

Figure 6: Capacity vs. number of rays for Location 18. Rays have been sorted in descending amplitude, and channel capacity is computed for spherical basis reconstructions with only the first n rays.